

Supporting Information for

Force-Dependent Structural Changes of Filamin C Rod Domains Regulated by Filamin C Dimer

Yunxin Deng¹ and Jie Yan^{1,2,3*}

¹*Mechanobiology Institute, National University of Singapore, Singapore 117411, Singapore*

²*Department of Physics, National University of Singapore, Singapore 117542, Singapore*

³*Joint School of National University of Singapore and Tianjin University, International Campus of Tianjin University, Binhai New City, Fuzhou, 350207, China*

Corresponding Author

*Jie Yan. Email: phyyj@nus.edu.sg

This Supporting Information file includes:

Supporting Information S1: Single-molecule construct sequence design.

Supporting Information S2. Single-molecule construct protein expression.

Supporting Information S3. Single-molecule construct working environment.

Supporting Information S4. Physiological force-loading rates.

Supporting Information S5. Illustration of transitions in the FLNC R24 dimer.

Supporting Information S6. Dwell time measurements of the FLNC R24 dimer under three additional forces.

Supporting Information S7. Bell's model fitting of force-dependent dissociation rates.

Supporting Information S8. Bootstrapping of recorded dwell times of FLNC R24 dimers under constant forces.

Supporting Information S9. Calculation of released contour length based on the unfolding step size of FLNC Ig-like repeats.

Supporting Information S10. FLNC rod-2 domain unfolding events at 23 °C.

Supporting Information S11. Sample size of recorded unfolding events of rod-1 and rod-2 domains.

Supporting Information S12. The physiological importance of tension duration over seconds timescale

Supporting Information S13. Force-dependent activation and the high-force deactivation of FLNC rod-2 domains.

References

Supporting Information S1. Single-molecule construct sequence design.

FLNC R24 dimer: spy-I27-I27-R24-Linker-avi-thrombin site-R24

AHIVMVDAYKPTKGGGSGLIEVEKPLYGVEVVFVGETAHFEIELSEPDVHGQWKL
KGQPLAASPDAEIIEDGKKHILILHNAQLGMTGEVSFQAANTKSAANLKVKELGG
GSGLIEVEKPLYGVEVVFVGETAHFEIELSEPDVHGQWKLKGQPLAASPDAEIIEDG
KKHILILHNAQLGMTGEVSFQAANTKSAANLKVKELGGGSGKLFSSDASKVVT
RGPGLSQAQFVGVQKNSFTVDCSKAGTNMMMVG VHGPKTPCEEVYVKHMGNRV
YNVTYTVKEKGDYILIVKWGDESVPGPSFKVKVEFGSGSSGSGSGSSGSGSSG
SGSSGSGSSGSSGSSGSGSGSSGSGSSGSSGSSGSSGSSGSSGSSGSSGSSGSSG
ESGSGSSGSGSGSSGSGSSGSGSSGSGSSGSSGSSGSSGSSGSSGSSGSSGSSGSSG
SGSSGSSGSGSGSSGSGSSGSSGSSGSLNDIFEAQKIEWHEGTGGGSGLVPRGSKFSS
DASKVVTRGPGLSQAQFVGVQKNSFTVDCSKAGTNMMMVG VHGPKTPCEEVYVK
HMGNRVYNVTYTVKEKGDYILIVKWGDESVPGPSFKVKV

FLNC R1 to R8 rod domains: thrombin site-avi-R1-R2-R3-R4-R5-R6-R7-R8-spy

LVPRGSGLNDIFEAQKIEWHEGTGGGSGSKQLNPCKAIA YGPGIEPQGNTVLQPA
HFTVQTV DAVGEVLVYIEDPEGHTEEAKVVPNNDKDRTYAVSYVPK VAGLHK
VTVLFAGQNIERSPFEVNVGMALGDANKVSARGPGLPVG NVANKPTYFDIYTA
GAGTGDVA VVIVDPQRRDTVEVALEDKGDSTFRCTYR PAMEGPHTVHVAFAG
APITRSPFPVHVSEACNPNACRASGRGLQPKGVRVKEVADFKVFTKGAGSGELK
VTVKGPKGTEEPVKVREAGDGVFECEYYPVVPGKYVVTITWGGYAI PRSPFEVQ
VSPEAGVQKVRAWGPGLTGGQV GKSADFVVEAIGTEVGT LGFSIEGPSQAKIECD
DKGDGSCDVRYWPTEPGEYAVHVICDDEDIRDS PFIAHILPAPPDCFPDKVKA FG
PGLPTGCIVDKPAEFTIDARAAGKGD LKLYAQDADGCPIDIKVIPNGDGTFRCS
YVPTKPIKHTIIISWGGVNVPKSPFRVNVGEGSHPERVKVYGP GVEKTGLKANEP
TYFTVDCSEAGQGDV SIGIKCAPGVVGP AEADIDFDIKN DNDTFTVKYTPPGAG
RYTIMVLFANQEIPASPFHIKVDPSHDASKVKAEGPGLNRTGVEV GKPTHFTVLT
KGAGKAKLDVQFAGTAKGEVVRDFEIIDNH DYSYTVKYTAVQQGNMAVTVY
GGDPVPKSPFVVNVAPPLDSLKIKVQGLNSKVA VQGQAFSVNTRGAGGQQL
DVRMTSPSRRPIPCKLEPGGGAEAQAVRYMPPEEGPYKVDITYDGHPVPGSPFAV
EGGGGSGAHIVMVDAYKPTK

FLNC R9 to R15 rod domains: thrombin site-avi-R9-R10-R11-R12-R13-R14-R15-spy

LVPRGSGLNDIFEAQKIEWHEGTGGGSGVLPPDPSKVCA YGPGGLKGGVLGTPAPF
SIDTKGAGTGGLGLTVEGPCEAKIECQDNGDGSCAVSYLPTEPGEYTINILFAEAH
IPGSPFKATIRPVFDPSKVRASGPGLERGKVGEAATFTVDCSEAGEAELTIEILSDA
GVKAEVLIHNNADGTYHITYSPA FPGTYTITIKYGGHPVPKFPTRVHVQPAVDTS
GVKVS GPGVEPHGVLREVTTEFTVDARSLTATGGNHVTARVLNPSGAKTDTYVT
DNGDGT YRVQYTAYEEGVHLVEVLYDEVA VPKSPFRVGVTEGCDPTRVRAFGP
GLEGLVNKANRFTVETRGAGTGGLGLAIEGPSEAKMSCKDNKDG SCTVEYIPF

TPGDYDVNITFGGRPIPGSPFRVPVKDVVDPGKVKCSGPGLGAGVRARVPQTFTV
DCSQAGRAPLQVAVLGPTGVAEPVEVRDNGDGTHTVHYTPATDGPYTVAVKYA
DQEVPRSPFKIKVLPAMDASKVRASGPGLNASGIPASLPVEFTIDARDAGEGLLV
QILDPEGKPKKANIRDNGDGTYYTVSYLPDMSGRYTITIKYGGDEIPYSPFRIHALP
TGDASKCLVTVSIGGHGLGACLGPRIQIGQETVITVDAKAAGEGKVTCTVSTPDG
AELDVDVVENHDGTFDIYYTAPEPGKYVITIRFGGEHIPNSPFHVLAGGGSGAHIV
MVDAYKPTK

FLNC R16 to R23 rod domains: thrombin site-avi-R16-R17-R18-R19-R20-R21-R22-R23-spy

LVPRGSGLNDIFEAKKIEWHEGTGGGSGPGARPTHWATEEPVVPVPEMESMLRP
FNLVIPFAVQKGELTGEVRMPSGKTARPNITDNKDGTITVRYAPTEKGLHQMGIK
YDGNHIPSPLQFYVDAINSRLHVSAYGPGLSHGVMNKPATFTIVTKDAGEGGLSL
AVEGPSKAEITCKDNKDGTCTVSYLPAPGDYSIIVRFDKHIPGSPFTAKITGDD
SMRTSQLNVGTSTDVSLKITESDLSQLTASIRAPSGNEEPCLLKRLPNRHIGISFTP
KEVGEHVSVRKSQKHVTNSPFKILVGPSEIGDASKVRVWGKGLSEGHTFQVAE
FIVDTRNAGYGGGLSIEGPSKVDINCEMEDGTCKVTYCPTEPGTYIINIKFADK
HVPSPFTVKVTGEGRMKESITRRRQAPSIATIGSTCDLNLKIPGNWFQMVSAQE
RLTRTFTRSSHTYTRTERTEISKTRGGETKREVRVEESTQVGGDPFPAVFGDFLGR
ERLGSFGSITRQQEAGEASSQDMTAQVTSPSGKVEAAEIVEGEDSAYSVRFPQEM
GPHTVAVKYRGQHVPSPFQFTVGPLGEGGAHKVRAGGTGLERGVAGVPAEFSI
WTREAGAGGLSIAVEGPSKAEIAFEDRDKDGSCGVSYYVQEPGDYEVSIFNDEHI
PDSFVVPVASLSDARRLTVTSLQETGLKVNQPASFAVQLNGARGVIDARVHT
PSGAVEECYVSELDSDKHTIRFIPHENGVHSIDVKFNGAHIPGSPFKIRVGEQSQ
GDPGLVSAYGPGLEGTTGVSSEFIVNTLNAGSGALSVTIDGPSKVQLDCRECE
GHVVTYTPMAPGNLYLAIKYGGPQHIVGSPFKAKVGGGSGAHIVMVDAYKPTK

Supporting Information S2. Single-molecule construct protein expression.

The protein expression and purification protocol involved the expression of all protein constructs in *E. Coli* DE3 with biotin protein ligase (BirA), followed by purification using a His-tag affinity column. To begin, the colonies transfected with the corresponding plasmids were precultured in 10 mL of LB medium with 100 $\mu\text{g mL}^{-1}$ ampicillin at 37 °C overnight. The precultures were then inoculated into 1 L of ampicillin-containing LB medium and grown at 37 °C until the optical density (OD_{600}) reached ~ 0.6 after approximately 4–6 hours. 0.4 mM IPTG and 50 μM biotin were then added to the cultures, and the resulting mixture was grown at 20 °C overnight. The biotin was catalyzed by BirA to conjugate to the avi-tag of proteins in the cell. Bacteria were harvested by centrifugation at 6000 g, and pellets were stored frozen at -80°C until further purification.

For the purification steps, bacterial pellets were resuspended with lysis buffer (50 mM Tris, 300 mM NaCl, pH=7.4) containing 1 mM PMSF, and the cells were mechanically lysed using French Press, followed by centrifugation at 40,000 g for 30 min. The resultant supernatants were allowed to bind to a Co^{2+} -NTA column (Thermo Scientific, DE, USA)

for 1 hour. After repeated washes using wash buffer (50 mM Tris, 300 mM NaCl, 10 mM imidazole, pH=7.4), the proteins were eluted into elution buffer (50 mM Tris, 300 mM NaCl, 200 mM imidazole, pH=7.4). These proteins were further purified using gel filtration chromatography (Superdex 200, Äkta Pure system, GE Healthcare, MA, USA). The protein-containing fractions were verified using SDS–polyacrylamide gel electrophoresis, dialyzed into PBS buffer, and frozen in aliquots with 15% (v/v) glycerol by liquid nitrogen for storage at $-80\text{ }^{\circ}\text{C}$.

Supporting Information S3. Single-molecule construct working environment.

The adhesion complex-containing recombinant proteins were prepared for sample analysis by diluting them to approximately 1 nM using the standard working buffer. This buffer consisted of 1 \times PBS, 1% (m/m) BSA, 1 mM DTT, and 0.1% Tween 20. To prepare the spy-catcher-functionalized channel for the experiment, it was washed several times with the same buffer. Next, the diluted proteins containing the spy-tag were introduced into the channel and incubated for 30 minutes to allow for the surface anchorage of the recombinant protein to the channel surface via spy-tag–spy-catcher interaction. The channel was then washed two times to remove any unbound proteins. After this, the experimenters added an appropriate amount of neutravidin-coated superparamagnetic beads into the channel and allowed them to incubate for 10 minutes. Finally, to avoid any effects of solution evaporation during the experiment, the channel was sealed using mineral oil. The sealed channel was then transferred and mounted onto the magnetic-tweezer setup to proceed with the experiment.

Supporting Information S4. Physiological force-loading rates.

Several factors determine the physiological force loading rate of filamin C (FLNC). The rigid body size of an Ig-like domain is approximately 5 nm ($b \approx 5\text{ nm}$), so it takes approximately $\frac{k_{BT}}{b} \sim \text{pN}$ of force to align the orientation of the Ig-like domains along the direction of stretching when a FLNC domain is in a force-transmission pathway. This results in an extension change of roughly 120 nm (or 24 domains \times 5 nm per domain) for the entire FLNC rod with folded domains. This extension change is similar in magnitude to the extension change of the I-band titin in the sarcomere between the resting phase and ventricular relaxation, which occurs over a time scale of approximately 0.5 seconds. Therefore, an estimated loading rate of a few pN per second is a reasonable approximation for the loading rate of FLNC over a large extension change range during heartbeats.

Our study shows that at this loading rate, the weak rod-2 domains of FLNC begin to unfold, providing additional buffering of forces up to a few pNs within an additional extension change of up to 100 nm (5 Rod-2 domains preceding the membrane-bound R21 \times 20 nm extension change per domain unfolding at a few pN forces), assuming, for example, that R21 is engaged with the integrin tail and the preceding 5 domains (R16 to R20) are unfolded. An illustration diagram showing the stretch-induced orientation of the FLNC Ig domains and unfolding is provided below (Figure. S1).

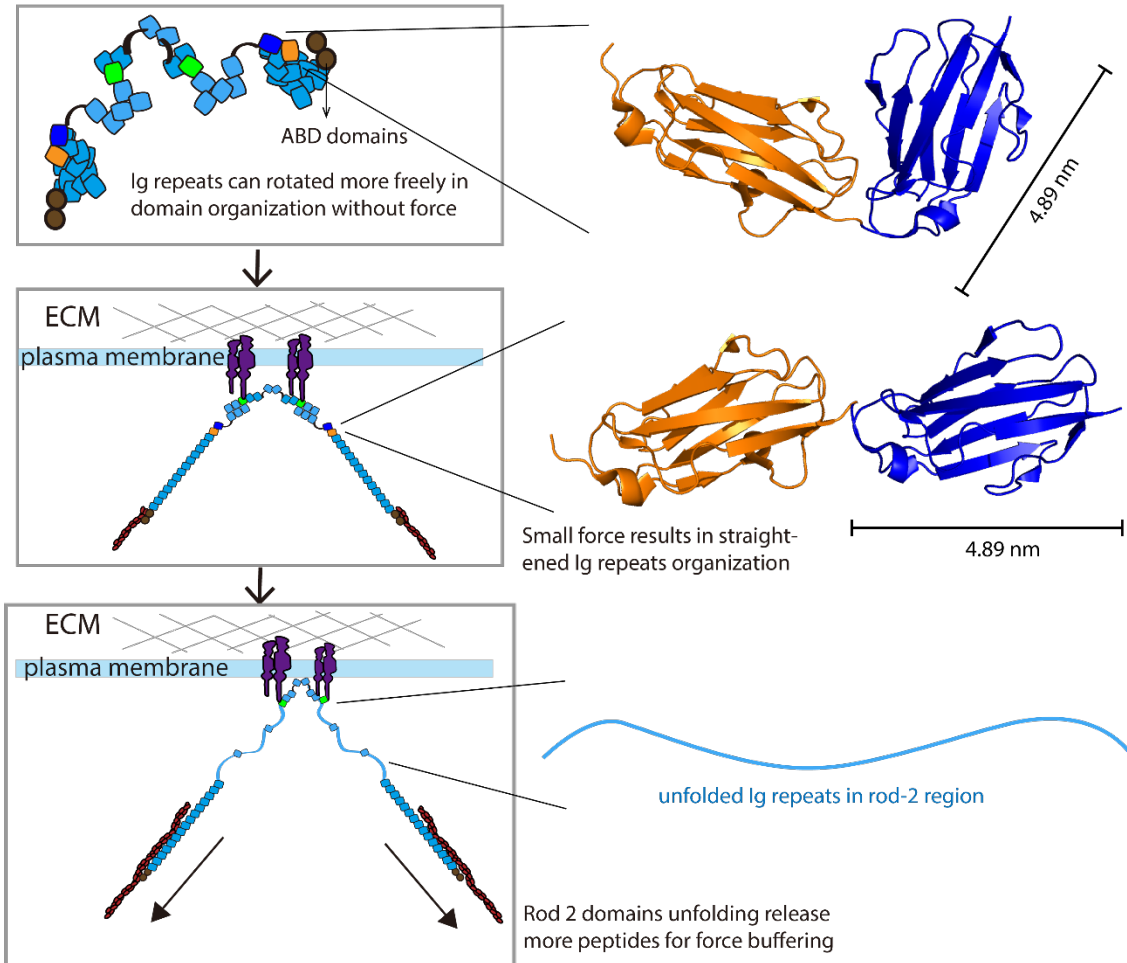


Figure S1. The FLN Ig-like domains exhibit initial random orientations, but they are aligned along the direction of stretching under small forces when FLN is involved in a force-transmission pathway. As the applied force increases, some domains located between the actin and membrane receptor binding domains can undergo unfolding, providing additional extension and buffering forces.

Supporting Information S5. Illustration of transitions in the FLNC R24 dimer.

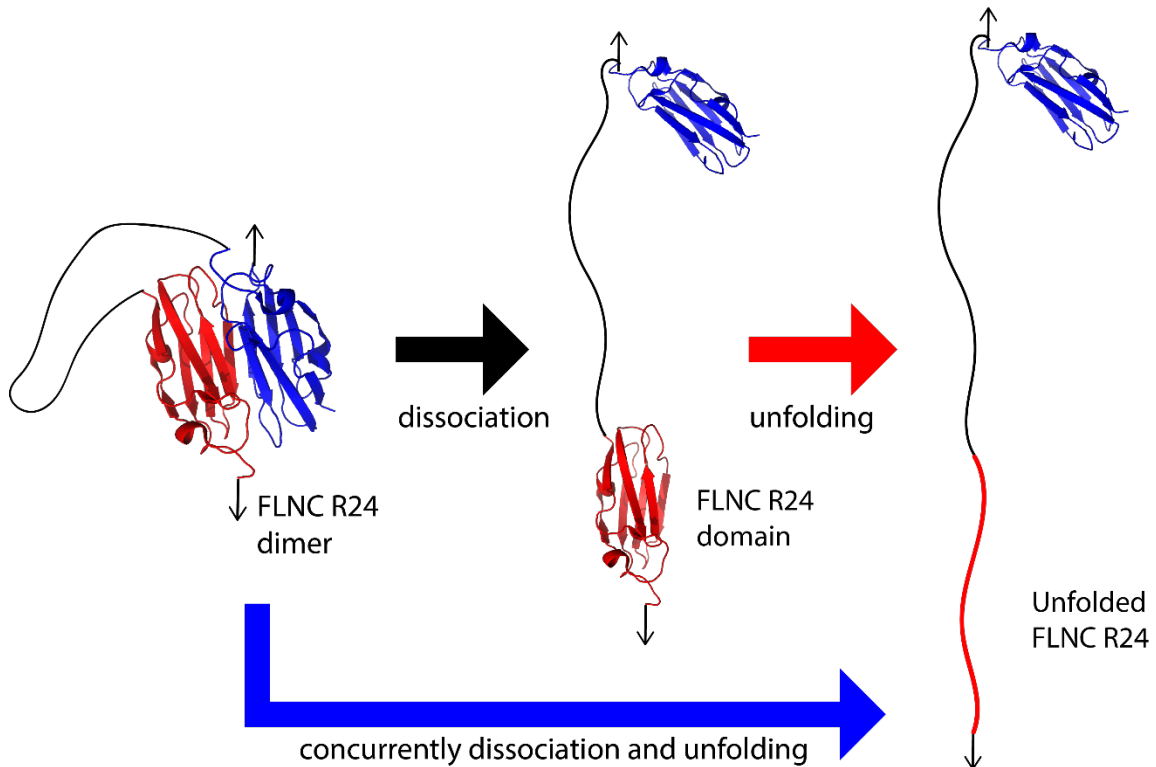


Figure S2. Transitions between three different states of the FLNC R24 dimer are depicted. The black arrow depicts the dissociation of the FLNC R24 dimer, which corresponds to the 3 pN and 8 pN conditions shown in figure 3a. The red arrow indicates the unfolding of a single FLNC R24 monomer after dissociation under force, corresponding to the second transition steps in figure S3a. The blue arrow represents the simultaneous dissociation and unfolding of one FLNC R24 domain, as seen under the 14 pN conditions in figure 3a.

Supporting Information S6. Dwell time measurements of the FLNC R24 dimer under three additional forces

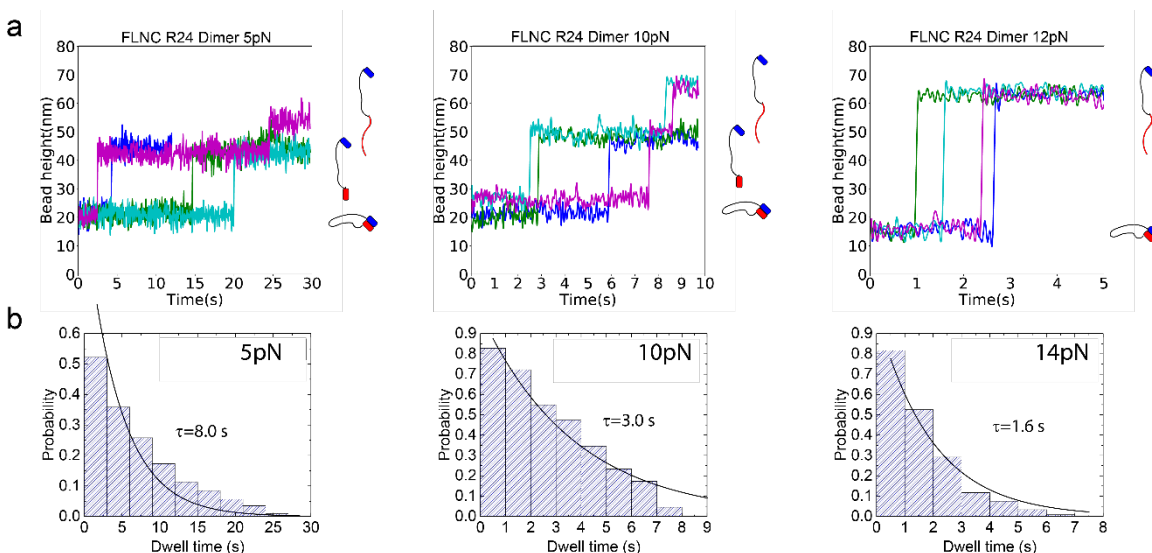


Figure S3. The dwell time measurements of R24 dimer at different forces. (a) The relationship between bead height and time for the FLNC R24 dimer is shown, with each cycle depicted in a different color. The zero time point marks the moment when the applied force transitions from 1 pN to the focused forces of 5 pN, 10 pN, and 12 pN. The right insets in each panel display the red and blue blocks representing the dissociated, associated, and combined dissociated and one unfolded R24 domain states of the FLNC R24 dimer. The double arrows indicate the recorded dwell time in each cycle. (b) The histogram of dwell times is shown, along with the fitted curve that was used to calculate the lifetime of the FLNC R24 dimer at the focused forces (represented as τ) through a single exponential decay.

Supporting Information S7. Bell's model fitting of force-dependent dissociation rates.

The force-dependent dissociation rates of FLNC R24 dimer can be determined from their force-dependent lifetimes, represented as $k(F) = 1/\tau(F)$. The force-dependent lifetimes and dissociation rates except 3 pN data point follow Bell's model curve as shown in the main text. Therefore, fitting the force-dependent dissociation rates $k(F)$ requires a single exponential function $k_0 e^{F\delta/k_B T}$, as shown in figure S4. The probability of FLNC R24 dimer dissociation forces under loading rate r can be calculated by $\rho(F) = \frac{k(F)}{r} e^{-\int_0^F \frac{k(f)}{r} df}$, where the integral at the exponential index, $\int_0^F k(f) df$, represents the area under the force-dependent curve (e.g. $\int_{0pN}^{12pN} k(f) df$ is shown in the grey area in figure S4).

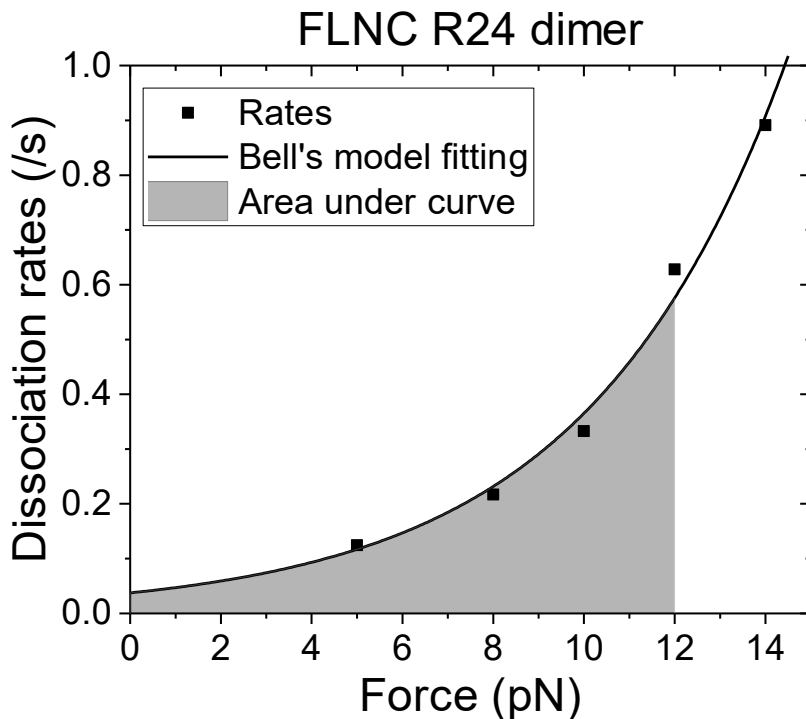


Figure S4. The figure shows the FLNC R24 dimer dissociation rates, denoted by squared points, which were calculated based on the dwell time distribution observed in experiments. The black solid curve represents Bell's model fitting. The area under the grey curve represents the integral of the rates from 0 to 12 pN.

Supporting Information S8. Bootstrapping of recorded dwell times of FLNC R24 dimers under constant forces.

With the recorded dwell times of FLNC R24 dimers, we applied bootstrapping sampling to the collected data of dwell times for 200 times and fitted the distribution of the dwell times with exponential decay function $e^{-t/\tau}$. This means that we will randomly select 200 samples from the original dataset with replacement, where each sample has the same size as the original dataset. After the bootstrap sampling, we got 200 lifetimes (τ) of FLNC R24 dimer at each force. We then calculated the statistics of interest (e.g. mean and standard deviation) for the 200 samples and plotted figure 4a with the mean lifetimes and their standard deviation.

Supporting Information S9. Calculation of released contour length based on the unfolding step size of FLNC Ig-like repeats.

Based on the worm-like chain model, the end-to-end distance of a flexible peptide follow the formula below

$$\frac{FA}{k_B T} = \frac{x}{L} + \frac{1}{4 \left(1 - \frac{x}{L}\right)^2} - \frac{1}{4}$$

A is the persistence length of peptide, which is usually 0.8 nm. F is the transition force where undimerization or unfolding occurs. x is the undimerization or unfolding step size, which is also the end-to-end distance of the linker or the unfolded Ig-like domain, respectively. In experiments, the transition force F and the step size x are obtained. Solving the equation, the contour lengths of the transitions can be calculated, which give the contour length values in the y-axis of figure 5 and 6.

Supporting Information S10. FLNC rod-2 domain unfolding events at 23 °C.

The reason why clear unfolding steps are not observed in the recorded data for rod-2 domains in figure. 7 is due to their intrinsic properties. These domains not only unfold at low forces (pN) at our loading rates but also undergo rapid unfolding and refolding transitions around their critical forces, making it difficult to capture clear steps at our limited sampling rate.

To observe clear steps, it is necessary to slow down the reversible transitions around the critical forces of these domains. We achieved this by reducing the temperature to ambient temperature (23 °C) during the revision. Clear steps were observed at this temperature, as demonstrated in Fig. S5. Since 23 °C is not a physiologically relevant temperature, we do not include the data in the main text. It is instead cited in the main text only when explaining the absence of clear unfolding steps at 37 °C.

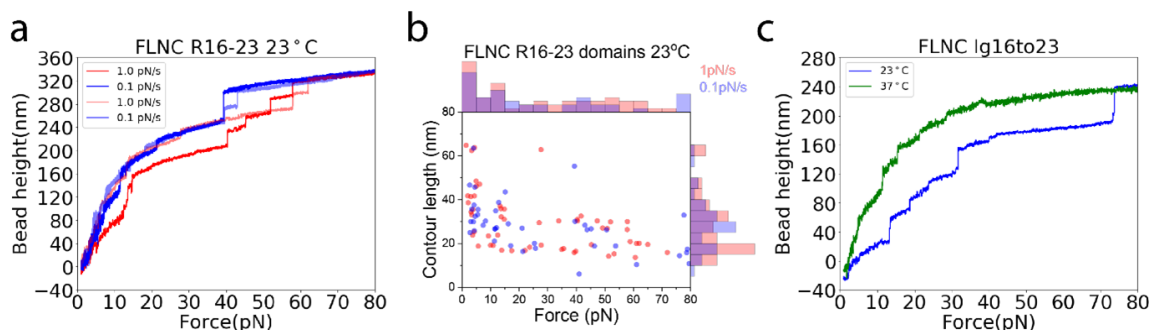


Figure S5. The analysis of the unfolding events of FLNC rod-2 domains under time-increasing forces at 23 °C. (a) Force versus bead height curves of FLNC rod-2 domains under time-increasing forces of 1 pN/s (red) and 0.1 pN/s (blue), with stepwise jump indicating domain unfolding events. (b) Distribution of unfolding forces and the corresponding contour length released with each step signal. (c) Comparison of force versus bead height curves of FLNC rod-2 domains at 23 °C and 37 °C.

Supporting Information S11. Sample size of recorded unfolding events of rod-1 and rod-2 domains.

For the R1-8 construct, the data of 10 pN/s are from 8 tethers, and the total number of stepwise signals detected are 85. The data of 1 pN/s are from 8 tethers, and the total number of stepwise signals detected are 57. The data of 0.1 pN/s are from 14 tethers, and the total number of stepwise signals detected are 194, but the figure. 5b only include randomly selected 80 from 194 to avoid overcrowding of the scatters.

For the R9-15 construct, the data of 10 pN/s are from 8 tethers, and the total number of stepwise signals detected are 57. The data of 1 pN/s are from 17 tethers, and the total number of stepwise signals detected are 85. The data of 0.1 pN/s are from 9 tethers, and the total number of stepwise signals detected are 86.

For the R16-23 construct with loading rate 1pN/s, we did more than 20 tethers, but not much clear stepwise signals were observed. Therefore, we cannot draw an unfolding force histogram like the rod-1 domains. The 23 °C data with loading rate 1pN/s are from 7 tethers, and the total number of stepwise signals detected are 61. The 23 °C data with loading rate 0.1 pN/s are from 7 tethers and the total number of stepwise signals detected are 44.

Supporting Information S12. The physiological importance of tension duration over seconds timescale

The time scale on the order of seconds appears to be critical in mechanotransduction. The significance of a few seconds lifetime over pN forces lies in two reasons: First, pN forces are necessary to activate mechanosensing domains in various mechanosensing proteins, such as talin rod domains ¹, α -catenins ^{2,3} and FLNC rod-2 domains shown in this study, which requires seconds to reach at physiologically relevant loading rate in the order of pN per second. Second, the binding of signaling proteins to the activated mechanosensing proteins takes time. In aqueous solutions, typical diffusion-limited binding rates range from $10^7 - 10^9 \text{ M}^{-1} \text{ s}^{-1}$. However, in cells, the binding rate is typically one to two orders of magnitude lower due to the crowded environment. Therefore, in μM concentrations, the binding time scale associated with binding takes seconds or longer.

The importance of the seconds time scale is also manifested from live cell experiments. For instance, the recently developed DNA-based tension gauge tethers are used to examine the minimal mechanical stability required for downstream mechanotransduction to occur in extracellular force-transmission linkages ⁴. In the case of integrin-based rigidity sensing of the extracellular matrix, a TGT that offers the minimal stability for integrin-based ECM rigidity sensing has a lifetime of a few seconds at 37°C under physiological forces of a few pN or under force-loading with a loading rate of a few pN/s. Similarly, TCR-ligand association requires the ability to withstand pN forces for seconds to facilitate T-cell activation ⁵.

Supporting Information S13. Force-dependent activation and the high-force deactivation of FLNC rod-2 domains.

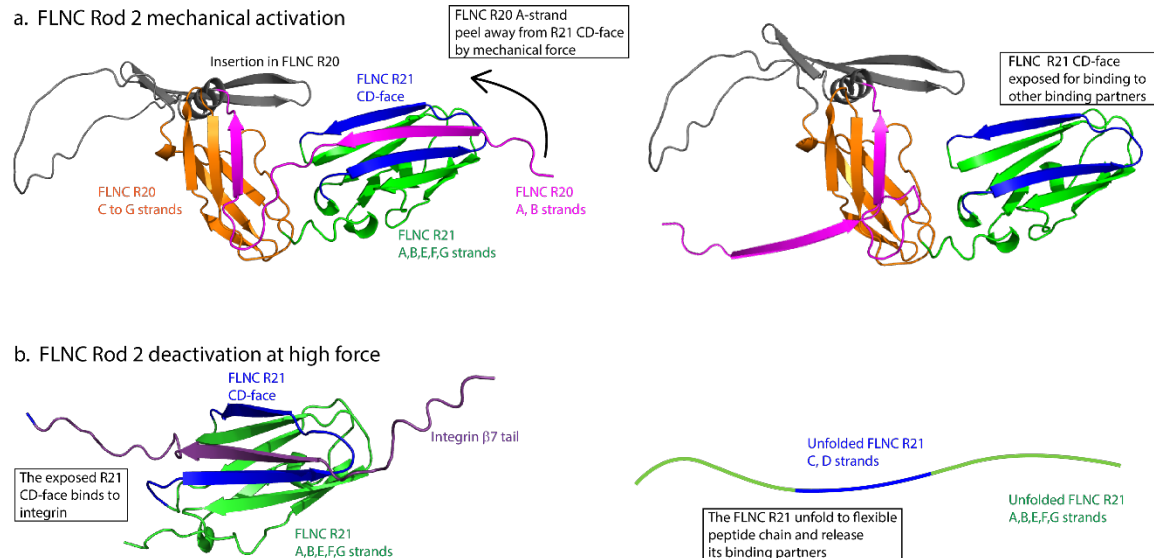


Figure S6. The mechanism of FLNC R20-21 pair in rod-2 region for mechanically activating and deactivating binding interactions with FLNC binding partners. The structure is provided by AlphaFold2 prediction.⁶ (a) Under sufficient mechanical force presumably of a few pN based on previous FLNA studies⁷, the FLNC R20-21 pair is activated as the A-strand of R20 is peeled away from the CD-face of R21, which exposes the binding sites on R21 for FLNC binding partners. (b) Further increased forces could cause the unfolding of the FLNC R21 domain, leading to the disruption of the FLNC R21 CD-face and release of binding partners from FLNC.

REFERENCES

- (1) Yao, M.; Goult, B. T.; Klapholz, B.; Hu, X.; Toseland, C. P.; Guo, Y.; Cong, P.; Sheetz, M. P.; Yan, J. The Mechanical Response of Talin. *Nat. Commun.* **2016**, *7* (May), 11966.
- (2) Yao, M.; Qiu, W.; Liu, R.; Efremov, A. K.; Cong, P.; Seddiki, R.; Payre, M.; Lim, C. T.; Ladoux, B.; Mège, R.-M.; Yan, J. Force-Dependent Conformational Switch of α -Catenin Controls Vinculin Binding. *Nat. Commun.* **2014**, *5*, 4525.
- (3) Pang, S. M.; Le, S.; Kwiatkowski, A. V.; Yan, J. Mechanical Stability of AT-Catenin and Its Activation by Force for Vinculin Binding. *Mol. Biol. Cell* **2019**, *30* (16), 1930–1937.
- (4) Liu, J.; Le, S.; Yao, M.; Huang, W.; Tio, Z.; Zhou, Y.; Yan, J. Tension Gauge Tethers as Tension Threshold and Duration Sensors. *ACS Sensors* **2023**, *8* (2), 704–711.
- (5) Hong, J.; Ge, C.; Jothikumar, P.; Yuan, Z.; Liu, B.; Bai, K.; Li, K.; Rittase, W.; Shinzawa, M.; Zhang, Y.; Palin, A.; Love, P.; Yu, X.; Salaita, K.; Evavold, B. D.; Singer, A.; Zhu, C. A TCR Mechanotransduction Signaling Loop Induces Negative Selection in the Thymus. *Nat. Immunol.* **2018**, *19* (12), 1379–1390.
- (6) Mirdita, M.; Schütze, K.; Moriwaki, Y.; Heo, L.; Ovchinnikov, S.; Steinegger, M. ColabFold: Making Protein Folding Accessible to All. *Nat. Methods* **2022**, *19* (6), 679–682.
- (7) Rognoni, L.; Stigler, J.; Pelz, B.; Yläñne, J.; Rief, M. Dynamic Force Sensing of Filamin Revealed in Single-Molecule Experiments. *Proc. Natl. Acad. Sci. U. S. A.* **2012**, *109* (48), 19679–19684.